Analytical description of the bending behaviour of NiTi shape-memory alloys

R. PLIETSCH*‡, C. BOURAUEL*, D. DRESCHER*, B. NELLEN‡
* *Department of Orthodontics and* ‡ *Department of Physics, University of Bonn, Germany*

Shape-memory alloys (SMA) exhibit "super-elastic" deformation behaviour in both tensile and bending tests: linear-elastic and ideal-plastic sections occur alternately during a load/unload cycle. A new analytical model for the description of pure bending of SMA on the background of continuum mechanics is given. This model allows mathematical derivation of elasticity parameters needed for the characterization of SMA deformation. The parameter set consists of six elastic moduli and three strain limits, leading to a total of nine mechanical quantities necessary for analytically setting up the associated bending moment/bending angle diagram. The physical relevance of the elasticity parameters delivered by the model is checked by comparing experimental and theoretical (computed on the base of the parameter set) force systems on a T-shaped spring.

1. Introduction

A linear section of a shape-memory wire displays a characteristic stress/strain behaviour ("super-elasticity") in tensile tests (Fig. 1): after a linear ascent in stress up to the strain limit ε_1, sharp bend follows. The deformation proceeds plateau-like with only a slight change in stress. Typical plateau widths for near equiatomic NiTi range from 4%–7% relative strain. The upper plateau strain limit is denoted by ε_2. Further loading causes another steep linear rise until the maximum strain, ε_{max}, is reached. Any violation of the elasticity limit, P, would result in irreversible deformation of the material, and eventually in rupture. The behaviour in unloading is similar: the curve can be subdivided into three linear sections characterized by an "unloading plateau" between the strain limits ε_3 and ε_4. However, this plateau is placed at a distinctly lower level, giving rise to a hysteresis in the graph. As any inflicted deformation (not exceeding the elasticity limit P) is non-plastic, the unloading branch ends close to the origin.

This extraordinary behaviour is caused by reversible transformations between austenitic and martensitic crystal phases [1–3]. In addition to thermal activation, these phase changes can be invoked by application of external mechanical stress (stress-induced martensite) [4]. Both variants play an important role in explaining the shape-memory effect [5–7].

Most recent investigations have concentrated on tensile or torsional properties of super-elastic alloys [8–10]. However, very few studies on the mechanical bending behaviour are available, although bending loads dominate in special medical devices such as endoscopes or orthodontic appliances where tooth movement is accomplished by using NiTi shape-memory alloys. This paper presents a consistent analytical model of pure bending on the background of continuum mechanics. Herewith, bending moment versus bending angle diagrams of super-elastic alloys can be mathematically derived from a given set of elasticity parameters. Vice versa, if a measured curve is provided, the material parameters of the alloy under investigation can be determined by using an adapted optimization and fit algorithm. As a proof of the mechanical and physical relevance of the parameters obtained from this procedure, they are used for the calculation of force systems generated by a T-shaped NiTi spring. On the other hand, these force systems can be measured directly with a force–torque sensor. A comparison of theoretical prediction and experimental data confirms the quality of the proposed model.

2. Analytical model of pure bending of super-elastic wires

The calculations involved in obtaining the bending moment, M, from given mechanical parameters will be presented in brief outlines only. Details can be found in the Appendix and [11].

2.1. Presuppositions

Like most theories, the analytical description of super-elastic bending needs several simplifying assumptions, most of which are suggested by stress/strain diagrams from tensile tests.

(i) The stress–strain behaviour is characterized by a combination of up to six linear elastic branches which can be described by Hooke's Law: $\sigma = \varepsilon E$ (see Fig. 1).

(ii) Any crystalline phase transformation is of reversible nature [3, 12].

(iii) The formation of stress-induced martensite is a continuous process between the strain limits, ε_1

(pure austenitic phase, no martensitic variants)/ε_2 (pure martensitic phase, transformation completed), and ε_3 (retransformation to austenite starts)/ε_4 (retransformation completed), respectively.

(iv) Any planes perpendicular to the wire cross-section (longitudinal planes) are stress-free. This assumption excludes all forms of transverse interactions (Kirchhoff–Love hypothesis).

(v) According to Fig. 2, the wire can be thought of being composed of infinitesimally thin, sandwich-like layers which do not interact mutually. Thus, when the wire is bent by an angle of 2α (where α denotes the rotation of one wire end with respect to the horizontal starting position), each layer defined by its thickness dz and vertical position z is exposed to a characteristic stress which is independent of the wire width. At $z = 0$ (half of the wire height), there is a stress-free plane called the neutral fibre. Fig. 3 shows the front perspective of a wire under bending load. Aside from the neutral fibre, another general layer at height z is marked in. While the neutral fibre remains constant in length, l, during a bending process, all other layers are lengthened or shortened by an amount Δl depending on their z coordinates (Δl positive when the fibre is situated above the neutral fibre, Δl negative when situated below the neutral fibre, see Fig. 3). Simple geometrical relations lead to the result:

$$\frac{l + \Delta l}{l} = \frac{R + z}{R} \tag{1}$$

and therefore

$$\varepsilon \equiv \frac{\Delta l}{l} = \frac{z}{R} \tag{2}$$

Consequently, in the case of circular bending (R = const.), the strain of a particular layer is proportional to its position z above or below the neutral fibre, making ε and z equivalent parameters. This statement is illustrated in Fig. 3 where the stress distribution over the cross-section of a wire under bending load (maximum strain exceeds ε_2) is depicted: With increasing distance from the neutral fibre ($z = 0$) σ rises according to Fig. 1.

(vi) A common but unproved assumption is that the material responds symmetrically to elastic stretch and compression. Therefore, the layers at equal distance above and below the n.f. are subject to the same absolute value of stress.

The preceding discussion leads to a decomposition of the wire section into three different classes:

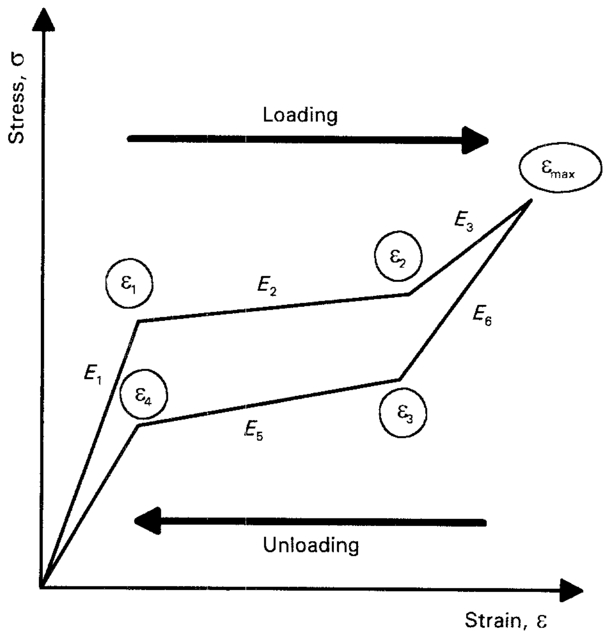

Figure 1 Stress/strain diagram typical of a shape-memory wire. The hysteresis curve can be decomposed into six linear-elastic sections.

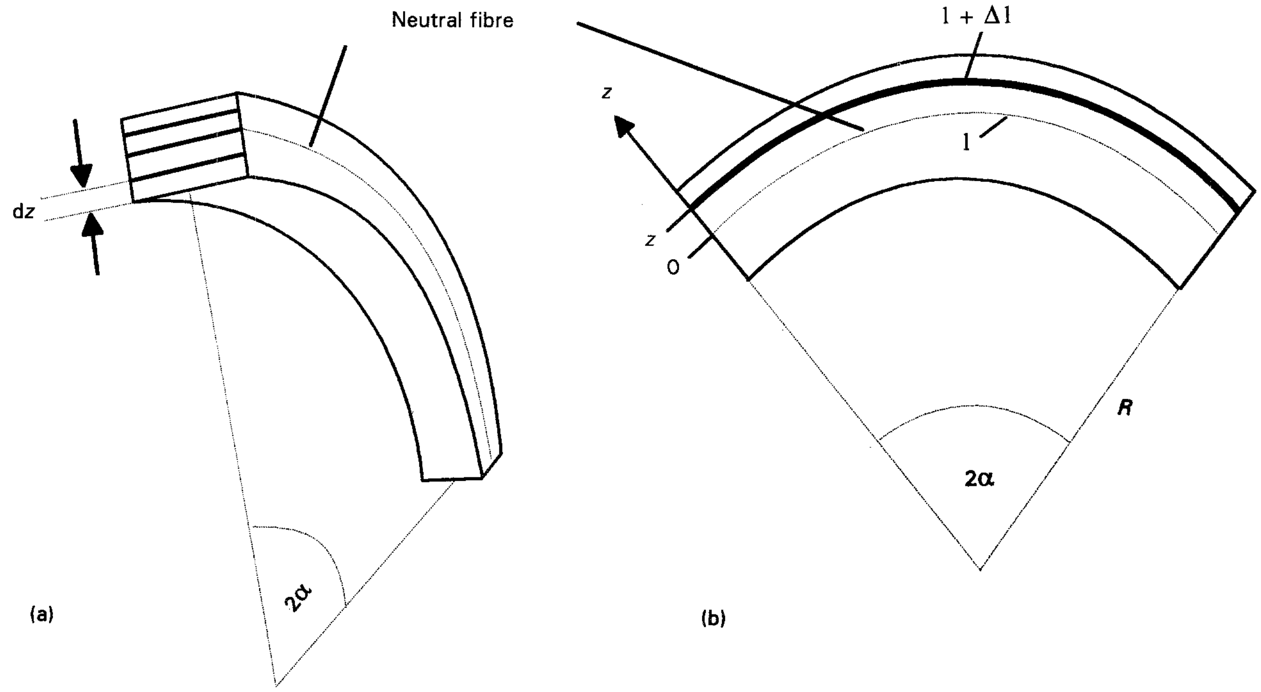

Figure 2 Decomposition of a wire into layers of quasi-constant stress for integration. The neutral fibre remains stress-free, all other fibres are exposed to z-dependent stress.

1. Class I comprises longitudinal layers of strain ranging from 0 to ε_1.

2. Class II contains fibres of strain between ε_1 and ε_2.

3. Class III covers a strain from ε_2 to ε_{max}, where ε_{max} denotes the maximum strain which is linked to the maximum bending angle

$$\varepsilon_{max} = \frac{z_{max}}{R_{min}} = \frac{h/2}{l/2\alpha_{max}} \tag{3}$$

Fig. 4 illustrates the generation of a moment by area force pairs (created by the underlying stress distribution) acting on a lever arm of length z. Correspondingly, the bending moment for a rectangular cross section yields

$$M = \int_A z F(A)\,\mathrm{d}A = 2\int_{A/2} z\sigma(A)\,\mathrm{d}A$$
$$= 2b \int_0^{h/2} z\sigma(z)\,\mathrm{d}z \tag{4}$$

where b is the wire width, h the wire height, $\sigma(z)$ the material stress at a height z above/below the neutral fibre.

Any calculations that will be presented hold for rectangular cross-sections only. However, they can be

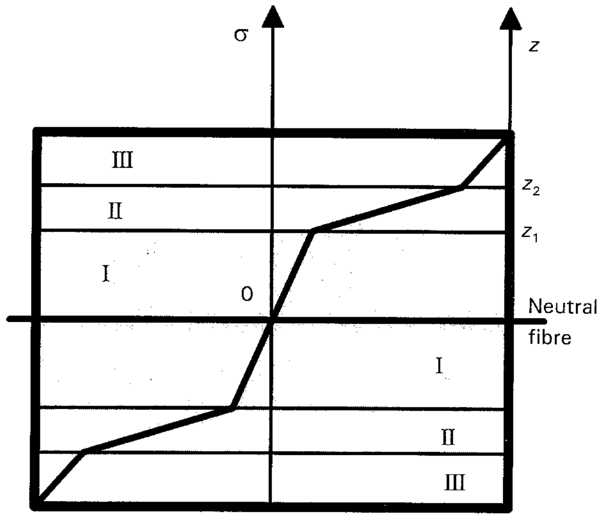

Figure 3 Stress distribution over a wire cross-section under bending deformation.

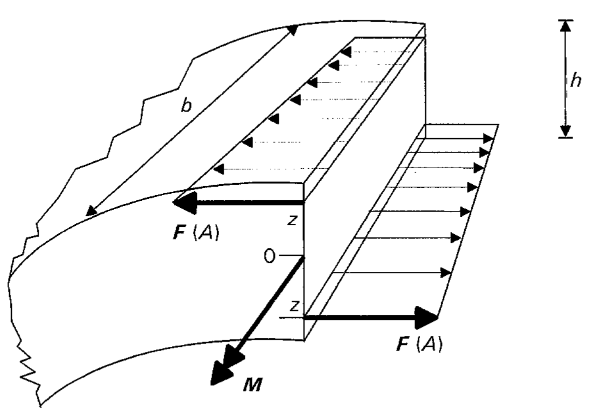

Figure 4 Generation of a bending moment by material stress. Area forces are responsible for the occurrence of a bending moment.

applied to round wires with slight modifications (use of trigonometrical functions) [12]. Because the expression $\sigma(z)$ is entirely different for loading and unloading directions, the procedure of integrating the total bending moment varies for both modes.

2.2. Moment integration for the loading mode

As mentioned before, the model describes non-linearity in the material behaviour by composing six linear sections. Thus, $\sigma(z)$ assumes a simple form, and the moment integration is trivial. Stress distributions and integral bending moments in loading mode are listed for the three classes I–III, respectively.

Class I (strain from 0 to ε_1)

$$\sigma_{\mathrm{I}}(z) = \varepsilon E_1 \tag{5}$$

$$M_{\mathrm{I}}(\alpha) = 2bE_1 \frac{z_1^3}{3R_\alpha} \tag{6}$$

Class II (strain between ε_1 and ε_2)

$$\sigma_{\mathrm{II}}(z) = \varepsilon_1 E_1 + (\varepsilon - \varepsilon_1)E_2 \tag{7}$$

$$M_{\mathrm{II}}(\alpha) = 2b\left[\varepsilon_1(E_1 - E_2)\frac{z_2^2 - z_1^2}{2} + E_2\frac{z_2^3 - z_1^3}{3R_\alpha}\right] \tag{8}$$

Class III (strain from ε_2 to ε_{max})

$$\sigma_{\mathrm{III}}(z) = \varepsilon_1 E_1 + (\varepsilon_2 - \varepsilon_1)E_2 + (\varepsilon - \varepsilon_2)(E_3 \tag{9}$$

$$M_{\mathrm{III}}(\alpha) = 2b\left\{\left[\varepsilon_1(E_1 - E_2) + \varepsilon_2(E_2 - E_3)\right] \times \frac{(h/2)^2 - z_2^2}{2} + E_3\frac{(h/2)^3 - z_2^3}{3R_\alpha}\right\} \tag{10}$$

The following abbreviations have been used:

$z_1 = \min(h/2, R_\alpha\varepsilon_1)$ z-coordinate of the specific layer, where ε_1 is reached;

$z_2 = \min(h/2, R_\alpha\varepsilon_2)$ z-coordinate of the specific layer, where ε_2 is reached;

$R_\alpha = 1/2\alpha$ radius of curvature; related to bending angle α.

The limitation of z_1 and z_2 to a maximum of $h/2$ is necessary to cancel the integrals M_{II} and/or M_{III} in cases where the bending angle is so small that these parts do not yet contribute to the integral.

The total bending moment in loading mode is the sum of the three class-specific partial moments: $M(\alpha) = M_{\mathrm{I}}(\alpha) + M_{\mathrm{II}}(\alpha) + M_{\mathrm{III}}(\alpha)$.

2.3. Moment integration for the unloading mode

Moment integration for the unloading mode is basically identical to the loading mode procedure. However, a major complication in the analytical treatment of the unloading direction is the fact that the development of a stress distribution in the wire cross-section is dependent on the loading history. Figs 5 and 6 illustrate the latter statement: when the maximum bending angle, α_{max}, is reached, strain values from 0–ε_{max}

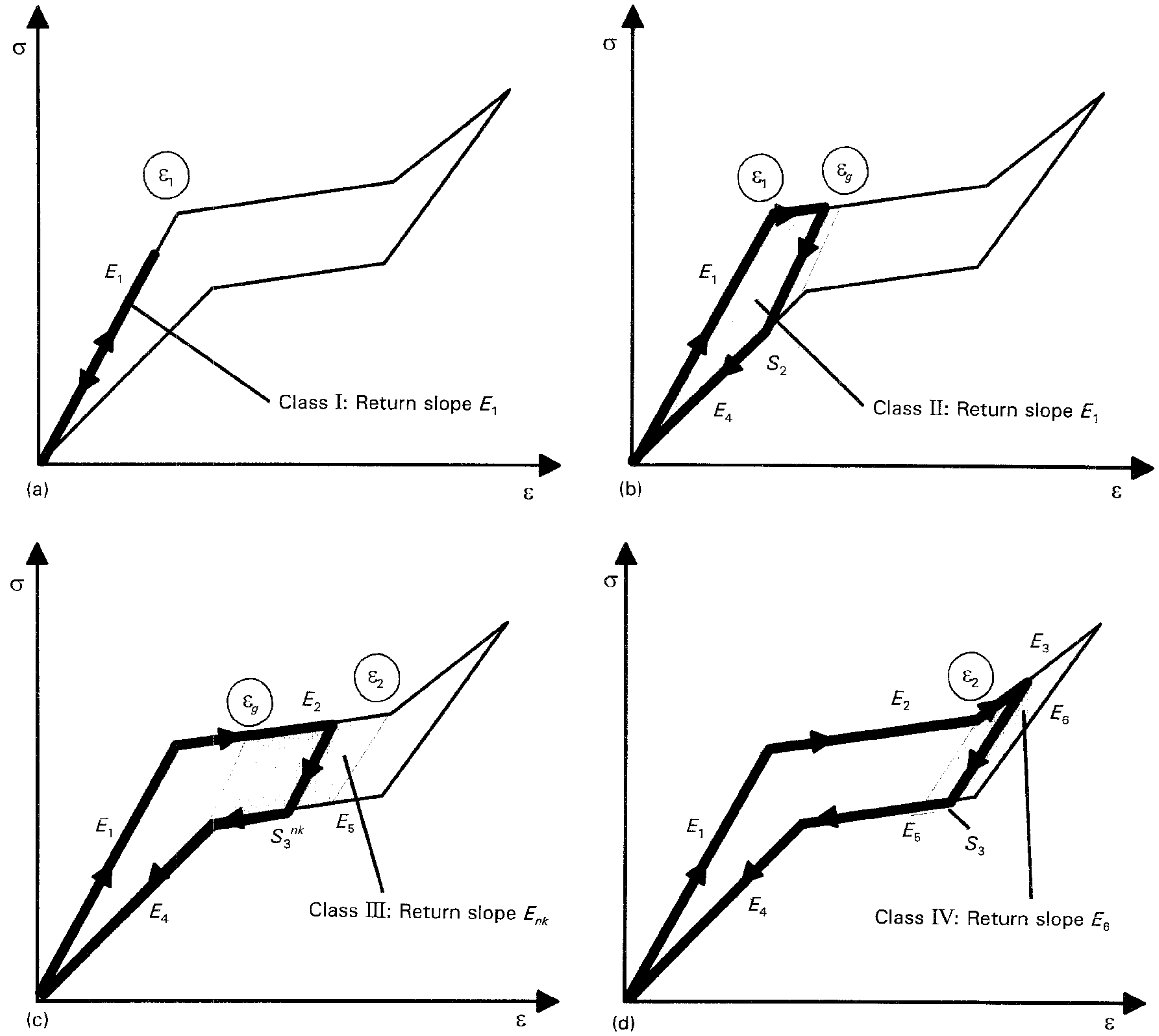

Figure 5 Stress diagrams for integration layers during a load/unload cycle: (a) Class I, (b) Class II, (c) Class III, (d) Class IV. Because the material behaviour is non-linear, the moment integration has to be divided into four classes, I–IV.

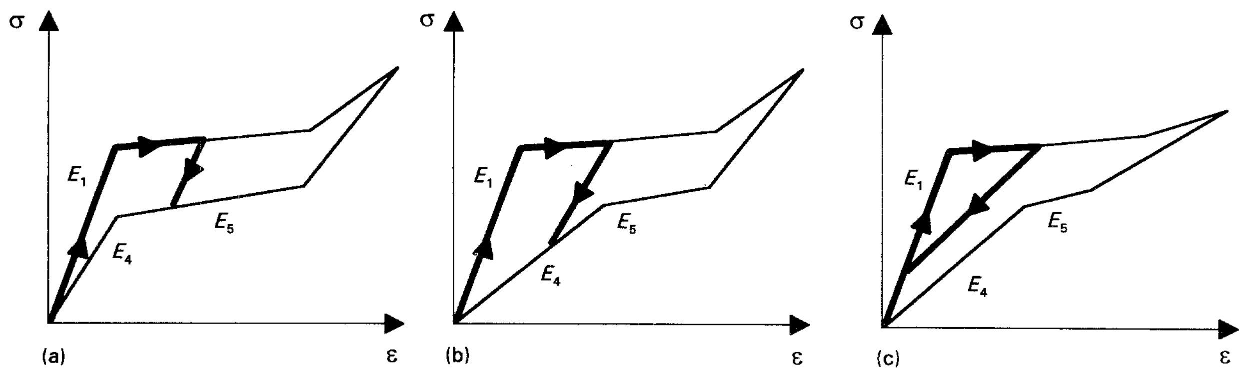

Figure 6 Possible stress curves of Classes II/III integration layers, depending on the set of elasticity parameters and the maximum stress in a specific fibre.

are distributed linearly (in sectors) over the z coordinate (see Fig. 3): the neutral fibre remains stress-free, fibres of Classes I–III are stretched up to certain limits.

2.3.1. Characterization and subdivision of integration classes in unloading

2.3.1.1. Class I. Fibres of maximum strain not exceeding ε_1 (Classs I, layers close to the neutral fibre) are treated as pure austenitic. They are untouched by martensitic transformations typically turning up at significantly higher strain levels. Therefore, they can be described by the Young's modulus of elastic austenitic deformation, E_1, which is equal for both loading and unloading mode (Fig. 5a). For a realistic choice of the parameter set (ε_i, E_i), the contribution of Class I layers to the total moment is of the order of a few percent.

2.3.1.2. Classes II/III. Any fibres of maximum strain values between ε_1 and ε_2 (plateau) undergo a stress-induced martensitic transformation and, incident to this phase change, a detwinning process which allows the material to display a pseudo-plastical behaviour [13]. Reasons for further decomposing these layers into Classes II and III will be explained later. The simplified model presented here assumes that the transformation is continuous and covers the whole plateau: at a maximum strain of ε_1 a fibre is purely austenitic, at ε_2 it is purely matensitic. For any maximum strain in between these limits, the fibre contains both phase variants to certain portions

$$\text{percentage of austenite} = \frac{\varepsilon_2 - \varepsilon_{\max}(z)}{\varepsilon_2 - \varepsilon_1} \tag{11}$$

$$\text{percentage of martensite} = \frac{\varepsilon_{\max}(z) - \varepsilon_1}{\varepsilon_2 - \varepsilon_1} \tag{12}$$

According to the phase portions, elasticity moduli between E_1 (slope of purely austenitic unloading, maximum strain ε_1) and E_6 (slope of purely martensitic unloading, maximum strain ε_2) have to be used

$$E[\varepsilon_{\max}(z)] = \frac{\varepsilon_2 - \varepsilon_{\max}(z)}{\varepsilon_2 - \varepsilon_1} E_1 + \frac{\varepsilon_{\max}(z) - \varepsilon_1}{\varepsilon_2 - \varepsilon_1} E_6 \tag{13}$$

$\varepsilon_{\max}(z)$ denotes the strain of an integration layer at a height z above the neutral fibre when the maximum bending angle is reached. As a result, every integration layer of Classes II/III has a different unloading slope depending on its maximum strain level. In turn, the maximum strain depends on the z coordinate of the fibre under consideration and therefore on the integration variable, preventing a simple analytical integration. However, the problem can be made integrable by the introduction of the following multi-group model.

Class II/III (maximum strain values from ε_1 to ε_2) integration layers are further subdivided into n groups with constant unloading slopes, respectively. The slope in group k is defined by

$$E_{nk} = \frac{(n - 1 - k)E_1 + kE_6}{n - 1}, \quad k = 1 \ldots n - 1. \tag{14}$$

Thus, the moment integral is split into n terms of a sum which can be evaluated analytically (see below). If the total number of subgroups n is large enough, a continuous slope change from E_1 to E_6 can be simulated.

As soon as a wire layer enters the lower plateau, E_5, a critical stress level is reached where martensite becomes thermodynamically unstable and austenite is the favoured phase [14]. Thus, the unloading branch follows the plateau (accompanied by a continuous phase change from martensitic to austenitic state) until the material has been completely retransformed to austenite (at ε_4). From there, it returns to the origin with a slope E_4 characteristic of austenitic unloading after transformation. This method of defining unloading slopes requires a distinction of different cases during the integration of stress for fibres with a maximum strain close to ε_1 depending on the choice of E_1, E_4, E_6 and ε_4 the unloading branch touches (a) the plateau, E_5, (b) the austenitic unloading branch, E_4, or (c) the austenitic loading branch, E_1. Fig. 6 shows these three possible situations.

To avoid this discrimination of three cases and to simplify the calculations further, Class II/III can be thought of as being composed of two distinct classes with well-defined returning slopes (explaining at the same time why the fibre class of maximum strain between ε_1 and ε_2 has been named II/III so long.

Class II is defined to comprise integration layers of strain values close to ε_1 and with an unloading branch which does not cross the lower plateau. For these layers, a uniform unloading slope E_1 is used (Fig. 5b). After the branch hits the austenitic return path, E_4, at a strain level S_2, it returns to the origin. The strain limit on the upper plateau, at which the according unloading branch does no longer hit the austenitic return path but the lower plateau is denoted by ε_g. Hence, any fibre of maximum strain between ε_1 and ε_g belongs to Class II. A significant change in the bending moment integral caused by using constant slopes over the whole range of Class II does not result, as the portion of Class II integrals in the total moment is in the order of a few per cent only.

Class III covers any fibres of maximum strain between ε_g and ε_2. Unloading branches intersect the plateau, E_5, at a strain limit, S_3^{nk}, In Class III, the slopes E_{nk} of the multi-group model apply (Fig. 5c). Despite the major volume of the wire layers belonging to Class III, their contribution to the integral bending moment during unloading is still small compared to Class IV (about 30% compared to 60%): because Class IV has a steep ascent (modulus E_3) large stress levels result. However, the situation is reversed in unloading. After a part of both Classes III/IV has reached the lower plateau, all stress per fibre values are in the same range making the larger volume portion of Class III the dominant criterion.

Class IV. Any fibres under a maximum strain greater than ε_2 belong to Class IV. According to the model, these layers are purely martensitic suggesting a slope of E_6 for the unloading branch. After hitting the plateau at a strain of S_4, the stress path continues with E_5 and E_4 towards the origin (Fig. 5d).

In the present study we have presupposed that four classes are sufficient to characterize the behaviour of all layers contained in the bent wire. As a consequence, the maximum strain must be restricted to 5%–8% in order to prevent irreversible plastic deformation which would not be covered by a description using four classes.

2.3.2. Bending moments in unloading

With the preceeding preparations, stress and bending moments can be evaluated. In this section, only the final results will be presented. Detailed derivations can be found in the Appendix and in [12]. Depending on the choice of elasticity parameters, two different events may occur in the calculations for Classes II, III and IV:

(a) fibres with higher z coordinates reach the intersection point $S_{2/3/4}$ first, lower z fibres follow, or

(b) fibres with lower z coordinates reach $S_{2/3/4}$ first, higher z fibres follow.

The relevance of this distinction is explained in the Appendix.

Class I (fibres of maximum strain between 0 and ε_1)

$$M_{\mathrm{I}}(\alpha) = 2b\frac{z_{01}^3 E_1}{3R_\alpha} \tag{14}$$

Class II (fibres of maximum strain between ε_1 and ε_g)

Case (a)

$$M_{\mathrm{II}}(\alpha) = 2b\left[\varepsilon_1(E_1 - E_2)\frac{z_2^2 - z_{01}^2}{2} + (E_2 - E_1)\frac{z_2^3 - z_{01}^3}{3R_{\min}} + E_1\frac{z_2^3 - z_{01}^3}{3R_\alpha} + E_4\frac{z_{0g}^3 - z_2^3}{3R_\alpha}\right] \tag{15}$$

Case (b)

$$M_{\mathrm{II}}(\alpha) = 2b\left[\varepsilon_1(E_1 - E_2)\frac{z_{0g}^2 - z_2^2}{2} + (E_2 - E_1)\frac{z_{0g}^3 - z_2^3}{3R_{\min}} + E_1\frac{z_{0g}^3 - z_2^3}{3R_\alpha} + E_4\frac{z_2^3 - z_0^3}{3R_\alpha}\right] \tag{16}$$

Class III (fibres of maximum strain between ε_g and ε_2)

Case (a)

$$\begin{aligned} M_{\mathrm{III}}(\alpha) = {} & 2b\sum_{k=0}^{n-1}\left[\varepsilon_1(E_1 - E_2)\frac{z_3^{nk2} - z_{nk}^2}{2} + (E_2 - E_{nk})\frac{(z_3^{nk})^3 - z_{nk}^3}{3R_{\min}} + E_{nk}\frac{(z_3^{nk})^3 - z_{nk}^3}{3R_\alpha}\right] \\ & + 2b\sum_{k=0}^{n-1}\left[E_4\frac{(z_z^{nk})^3 - (z_3^{nk})^3}{3R_\alpha} + \varepsilon_4(E_4 - E_5) \times\frac{z_{n,k+1}^2 - (z_z^{nk})^2}{2} + E_5\frac{z_{n,k+1}^3 - (z_z^{nk})^3}{3R_\alpha}\right] \end{aligned} \tag{17}$$

Case (b)

$$\begin{aligned} M_{\mathrm{III}}(\alpha) = {} & 2b\sum_{k=0}^{n-1}\left[\varepsilon_1(E_1 - E_2)\frac{z_{n,k+1}^2 - (z_3^{nk})^2}{2} + (E_2 - E_{nk})\frac{z_{n,k+1}^3 + (z_3^{nk})^3}{3R_{\min}} + E_{nk}\frac{z_{n,k+1}^3 - (z_3^{nk})^3}{3R_\alpha}\right] \\ & + 2b\sum_{k=0}^{n-1}\left[E_4\frac{(z_z^{nk})^3 - z_{nk}^3}{3R_\alpha} + \varepsilon_4(E_4 - E_5)\frac{(z_3^{nk})^2 - (z_z^{nk})^2}{2} + E_5\frac{(z_3^{nk})^3 - (z_z^{nk})^3}{3R_\alpha}\right] \end{aligned} \tag{18}$$

Class IV (fibres of maximum strain greater than ε_2)

Case (a)

$$\begin{aligned} M_{\mathrm{IV}}(\alpha) = {} & 2b\left\{[\varepsilon_1(E_1 - E_2) + \varepsilon_2(E_2 - E_3)]\frac{z_4^2 - z_{02}^2}{2} + (E_3 - E_6)\frac{z_4^3 - z_{02}^3}{3R_{\min}} + E_6\frac{z_4^3 - z_{02}^3}{3R_\alpha}\right\} \\ & + 2b\left\{E_4\frac{z_z^3 - z_4^3}{3R_\alpha} + \varepsilon_4(E_4 - E_5) \times\frac{(h^2/4) - z_z^2}{2} + E_5\frac{(h^3/8) - z_z^3}{3R_\alpha}\right\} \end{aligned} \tag{19}$$

Case (b)

$$\begin{aligned} M_{\mathrm{IV}}(\alpha) = {} & 2b\left\{[\varepsilon_1(E_1 - E_2) + \varepsilon_2(E_2 - E_3)]\frac{(h^2/4) - z_4^2}{2} + (E_3 - E_6)\frac{(h^3/8) - z_4^3}{3R_{\min}} + E_6\frac{(h^3/8) - z_4^3}{3R_\alpha}\right\} \\ & + 2b\left[E_4\frac{z_z^3 - z_{02}^3}{3R_\alpha} + \varepsilon_4(E_4 - E_5) \times\frac{z_4^2 - z_z^2}{2} + E_5\frac{z_4^3 - z_z^3}{3R_\alpha}\right] \end{aligned} \tag{20}$$

The total bending moment during the unloading process is the sum over all contributions of Classes I–IV

$$M(\alpha) = M_{\mathrm{I}}(\alpha) + M_{\mathrm{II}}(\alpha) + M_{\mathrm{III}}(\alpha) + M_{\mathrm{IV}}(\alpha) \tag{21}$$

3. Determination of elasticity parameters in bending experiments

Using the analytical model presented, bending moment/bending angle diagrams can be calculated for any given set of elasticity parameters (ε_i, E_i). Yet the aim of an evaluation routine for bending experiments is vice versa: elasticity parameters are to be derived from experimental moment/angle data which means the inversion of the moment integration and therefore is not trivial. An indirect, iterative least squares fit [15] provides a suitable solution: a set of start parameters is chosen to generate a moment/angle graph for a defineable number of different bending angles. This diagram is compared to the measured bending data, and deviations are squared and added. Furthermore, the gradient with respect to variation of the elasticity parameters is evaluated, thereby providing a correction in the start parameters necessary for better agreement. This correction is used for the next iteration step repeatedly until the least square value no longer changes noticeably (break-off criterion).

The evaluation program uses a modified Levenberg–Marquardt algorithm [16] with iterative stepwidth adaptation. Start values, number of different bending angles, number of groups (in the multi-group model) and break-off criteria can be defined as fit parameters. The theoretical fit curve is superposed with the experimental data to provide an additional visual comparison.

4. Verification of the model

An example moment curve of a super-elastic NiTi wire (Unitek* Nitinol SE®, rectangular cross-section 0.016 in × 0.022 in, $l = 8$ mm) is fitted to serve as a first test whether the simplified bending model allows an appropriate description of the bending mechanism with a set of nine parameters (ε_i, E_i). Fig. 7a shows the superposition of nine measurements with maximum bending angles of 10°, 20°, 30°, ..., 90°. Fig. 7b displays the result of the corresponding Marquardt fit. The curves are in excellent agreement, as the difference diagram (Fig. 7c) illustrates. In addition, the measured graphs (Fig. 7a) display exactly the same unloading behaviour as was used in the model: for small maximum load (10°–30° maximum bending angle), loading and unloading paths have approximately the same slope (E_1 in the σ/ε plot), and for increasing maximum angle they pass continuously into the martensite unloading slope (E_6 in the σ/ε plot). Therefore, the multi-group theory, decomposition into four moment classes and limitation to nine parameters are proven as adequate for a theoretical description of the bending behaviour of super-elastic wires.

Despite the satisfying congruence of theoretical and experimental moment curves, the physical relevance of the evaluated parameters is still questionable. To prove that the model describes the super-elastic bending mechanism satisfactorily, the parameter set will be employed for the calculation of a force system of an orthodontic T-shaped spring (T-loop) subject to an activating force. These calculations will be performed using a plane model of super-elasticity based on the finite element method (FEM). The model described elsewhere [17] enables the determination of the behaviour of NiTi shape-memory alloys and is capable of simulating large structural displacements

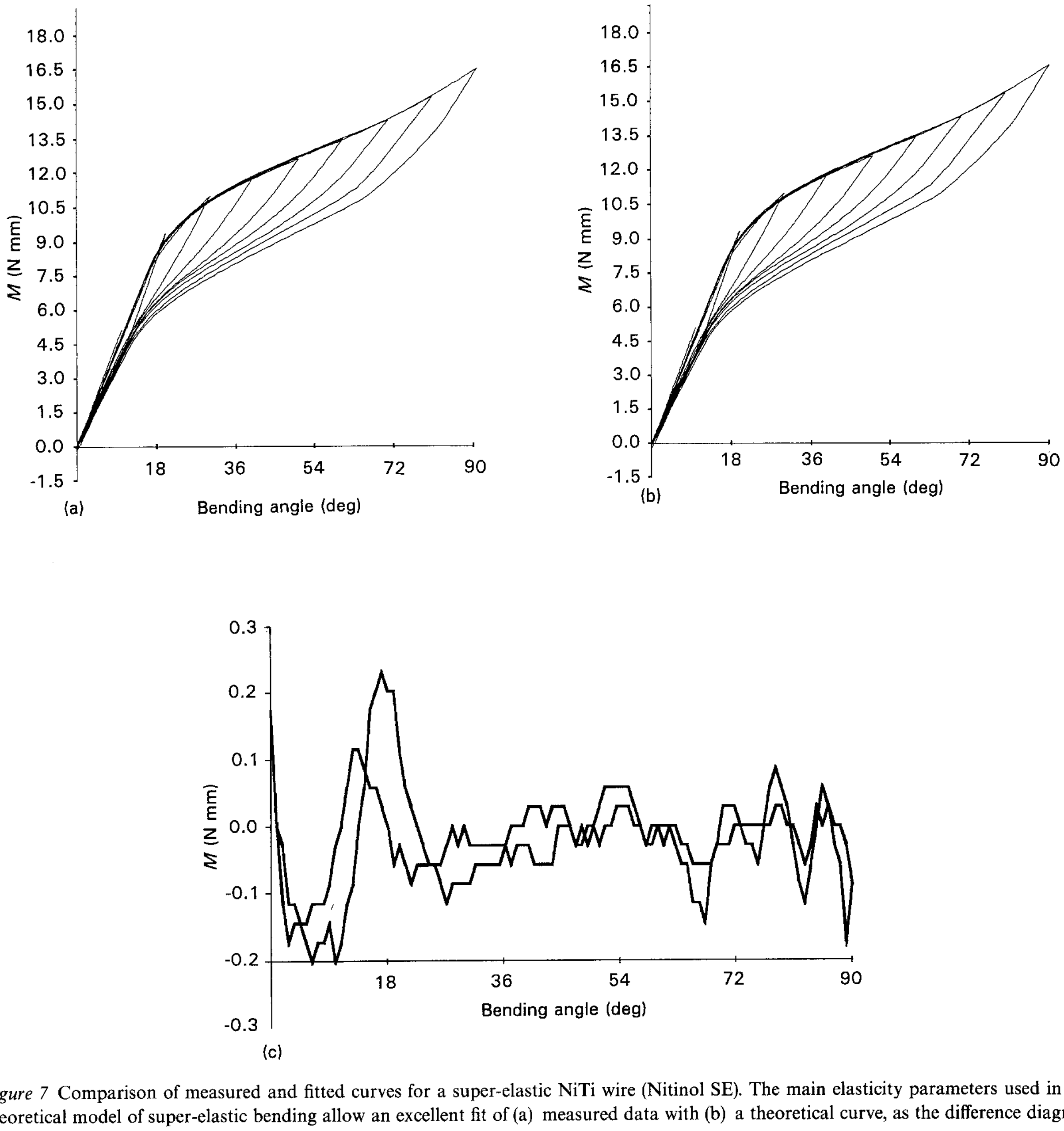

Figure 7 Comparison of measured and fitted curves for a super-elastic NiTi wire (Nitinol SE). The main elasticity parameters used in the theoretical model of super-elastic bending allow an excellent fit of (a) measured data with (b) a theoretical curve, as the difference diagram (c) shows.

*Unitek/3M, Monrovia, CA, USA.

and rotations accompanied by moderate strains (up to 10%). Using the nine mechanical parameters of super-elasticity described above, the FEM determines the non-linear stress/strain distribution in the cross-section of a planar beam and subsequently performs a numerical integration using a Gaussian Quadrature algorithm to calculate the force systems. The numerical results are compared with the force system of the T-loop measured directly by a three-dimensional force-torque sensor [18]. To simplify matters, only two dominant components of the measured and calculated force systems are depicted: the lateral force, F_x, and the moment, M_y (Fig. 8). Both force and moment are in good conformity with the calculations based on bending parameters (Fig. 9). The results of this study substantiate the whole analytical proceeding presented.

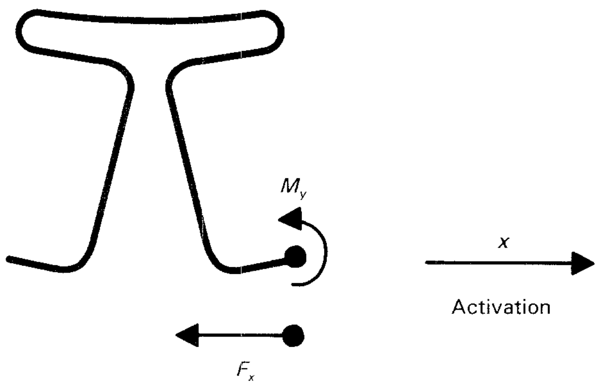

Figure 8 Force system of a plane T-loop. Dominant components are the lateral force, F_x, acting against the activation, and moment, M_y.

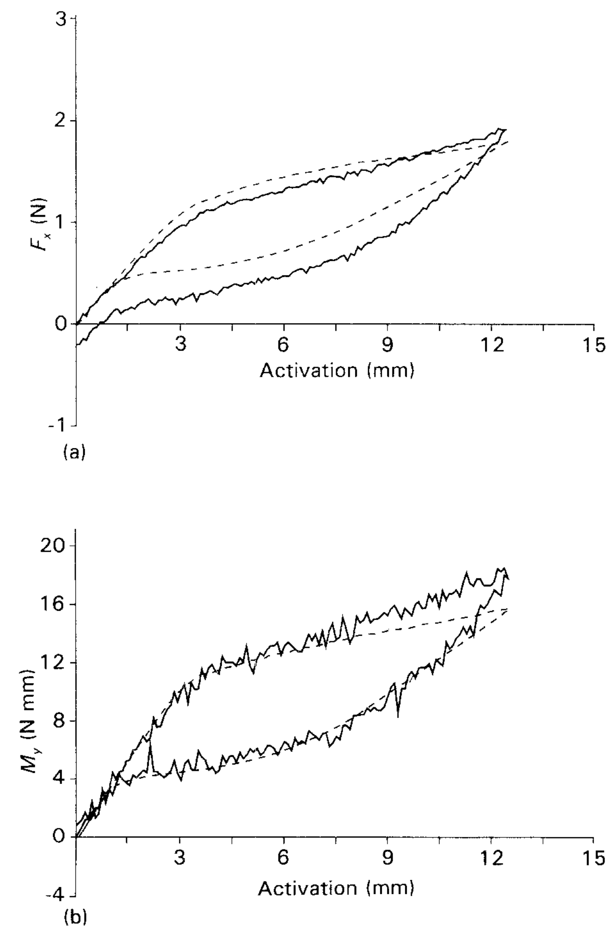

Figure 9 (a) (—) Measured and (- - -) calculated lateral force, F_x, on the T-spring. (b) (—) Measured and (- - -) calculated moment, M_y, on the T-spring.

5. Conclusion

NiTi memory wires display a characteristic material behaviour in bending experiments. The bending process can be described by a stress/strain curve linear by sectors. It is characterized by a set of nine parameters (ε_i, E_i) which are suggested by tensile tests. The moment integration requires a decomposition of the wire into classes and subclasses in order to make the calculations compatible with continuum mechanics. Not only does the model of super-elastic bending allow the calculation of moment/angle diagrams from given parameter sets, it reversely provides elasticity parameters relevant for the mechanical behaviour of the material with the aid of bending experiments.

Appendix

The moment integration in unloading is presented in detail here. However, trivial algebraic reformations have been omitted. The classification of wire fibres (Classes I–IV) in unloading was described earlier.

A.1. Class I (fibres of maximum strain between 0 and ε_1)

Unloading leads towards the origin with the uniform slope, E_1 (Fig. 5a). While wire fibres are classified by their maximum strain, the z coordinate relative to the neutral fibre is needed for moment calculations. Maximum strain between 0 and ε_1 is equivalent to z values from $z = 0$–$z = z_{01} \equiv \varepsilon_1 R_\alpha$. Thus, the integral for Class I may be written as (the integrands I_k^{Class} are defined as $I_k^{\text{Class}} \equiv 2bz\sigma_k^{\text{Class}}\text{d}z$. Further explanations are given in parentheses)

$$M_{\text{I}} = \int_0^{z_{01}} I_1^{\text{I}} \text{ (unloading path from } \varepsilon_{\max} \text{ to 0)} \qquad \text{(A1)}$$

The unloading path is characterized by a stress $\sigma_1^{\text{I}} = \varepsilon E_1$. Thus, the final result of integration yields

$$M_{\text{I}}(\alpha) = 2b\frac{z_{01}^3 E_1}{3R_\alpha} \qquad \text{(A2)}$$

A.2. Class II (fibres of maximum strain between ε_1 and ε_g)

The unloading path for Class II layers starts from ε_1, leads with constant slope E_1 towards the austenite unloading branch, E_4, which is crossed at a strain S_2 and continues towards the origin (Fig. 5b). ε_g is defined as the smallest strain on the loading plateau, from where unloading with E_1 still touches the unloading plateau. ε_g is determined by a "mesh" (closed path) in the stress/strain diagram

$$\varepsilon_1 E_1 + (\varepsilon_g - \varepsilon_1)E_2 = \varepsilon_4 E_4 + (\varepsilon_g - \varepsilon_4)E_1 \qquad \text{(A3)}$$

This leads to

$$\varepsilon_g = \varepsilon_1 + \varepsilon_4 \frac{E_4 - E_1}{E_2 - E_1} \qquad \text{(A4)}$$

The strain coordinate, S_2, of the intersection point where the unloading branch crosses the austenite return path (slope E_4) can be derived from a similar mesh in the σ/ε plot

$$\varepsilon_1 E_1 + (\varepsilon_{max} - \varepsilon_1)E_2 = S_2 E_4 + (\varepsilon_{max} - S_2)E_1 \quad (A5)$$

Replacing $\varepsilon_{max} = z/R_{min}$ yields S_2

$$S_2 = \left(\frac{z}{R_{min}} - \varepsilon_1\right)\frac{E_1 - E_2}{E_1 - E_4} \quad (A6)$$

As before, strains have to be translated into height coordinates for the purpose of integration. To obtain the z coordinate related to S_2 (for a given bending angle), S_2 is equated with z/R_α, the strain a fibre at z is exposed to at a bending angle α. This leads to

$$z_{S_2}(\alpha) = R_{min}\varepsilon_1 \bigg/ \left(1 - \frac{R_{min}}{R_\alpha}\frac{E_1 - E_4}{E_1 - E_2}\right) \quad (A7)$$

Because Class II z coordinates only contribute to the integral if they are related to strain values between ε_1 and ε_g, the following restrictions have to be made

$$z_2 \equiv \min[\max(z_{S_2}(\alpha), z_{01}], z_{0g} \quad (A8)$$

with $z_{01} \equiv R_{min}\varepsilon_1$ and $z_{0g} \equiv R_{min}\varepsilon_g$.

Introducing z_2 divides the Class II bending moment into two components:

(i) the moment generated by fibres that have not yet passed the strain limit S_2;

(ii) the moment produced by fibres which have already passed S_2 and now follow the austenite unloading branch, E_4, towards the origin.

Depending on the choice of elasticity parameters, two different events may occur:

(a) fibres with higher z coordinates reach S_2 first, lower z fibres follow, or

(b) fibres with lower z coordinates reach S_2 first, higher z fibres follow.

Therefore, the expression for S_2 has to be analysed for any set of parameters (ε_i, E_i) in order to decide if case (a) or (b) has to be employed for further calculations. Accordingly, two different Class II integrals are possible.

Case (a)

$$\begin{aligned} M_{II} &= \int_{z_{01}}^{z_{0g}} I^{II} \\ &= \int_{z_{01}}^{z_{S_2}} I_1^{II} \text{ (unloading branch from } \varepsilon_{max} \text{ to } S_2) \\ &+ \int_{z_{S_2}}^{z_{0g}} I_2^{II} \text{ (unloading branch from } S_2 \text{ to } 0) \end{aligned} \quad (A9)$$

Case (b)

$$\begin{aligned} M_{II} &= \int_{z_{01}}^{z_{0g}} I^{II} \\ &= \int_{z_{01}}^{z_{S_2}} I_1^{II} \text{ (unloading branch from } S_2 \text{ to } 0) \\ &+ \int_{z_{S_2}}^{z_{0g}} I_1^{II} \text{ (unloading branch from } \varepsilon_{max} \text{ to } S_2) \end{aligned} \quad (A10)$$

The corresponding stress expressions are given by

$$I_1^{II}: \sigma_1^{II} = \varepsilon_1 E_1 + (\varepsilon_{max} - \varepsilon_1)E_2 - (\varepsilon_{max} - \varepsilon)E_1 \quad (A11)$$

$$I_2^{II}: \sigma_2^{II} = \varepsilon E_4 \quad (A12)$$

so we finally have

Case (a)

$$M_{II}(\alpha) = 2b\left[\varepsilon_1(E_1 - E_2)\frac{z_2^2 - z_{01}^2}{2} + (E_2 - E_1) \times \frac{z_2^3 - z_{01}^3}{3R_{min}} + E_1\frac{z_2^3 - z_{01}^3}{3R_\alpha} + E_4\frac{z_{0g}^3 - z_2^3}{3R_\alpha}\right] \quad (A13)$$

Case (b)

$$M_{II}(\alpha) = 2b\left[\varepsilon_1(E_1 - E_2)\frac{z_{0g}^2 - z_2^2}{2} + (E_2 - E_1) \times \frac{z_{0g}^3 - z_2^3}{3R_{min}} + E_1\frac{z_{0g}^3 - z_2^3}{3R_\alpha} + E_4\frac{z_2^3 - z_{01}^3}{3R_\alpha}\right] \quad (A14)$$

A.3. Class III (fibres of maximum strain between ε_g and ε_2)

The unloading branch for Class III layers starts at a maximum strain, decreases with a slope E_{nk} which simulates the continuous transition from the Class I return slope E_1 to the Class IV slope E_6 in n steps (Fig. 5c):

$$E_{nk} = \frac{(n - k - 1)E_1 + kE_6}{n - 1}, \quad k = 0 \ldots n - 1.$$

These n steps are related to n groups of constant gradient, respectively. They are integrated separately and summed up. Every unloading branch (E_{nk}) hits the lower plateau at a group-dependent strain, S_3^{nk}, where it continues with slope E_5 until ε_4 is reached. It returns to the origin with E_4.

The intersection strain, S_3^{nk}, is again derived from a stress/strain mesh

$$\varepsilon_1 E_1 + (\varepsilon_{max} - \varepsilon_1)E_2 = \varepsilon_4 E_4 + (\varepsilon_{max} - S_3^{nk})E_{nk} + (S_3^{nk} - \varepsilon_4)E_5 \quad (A15)$$

Inserting $\varepsilon_{max} = z/R_{min}$ yields S_3^{nk}

$$S_3^{nk} = \frac{(z/R_{min})(E_2 - E_{nk}) + \varepsilon_1(E_1 - E_2) + \varepsilon_4(E_5 - E_4)}{E_5 - E_{nk}} \quad (A16)$$

The corresponding z coordinate on the loading branch is given by the equation

$$S_3^{nk} = \frac{z_{S_3}^{nk}(\alpha)}{R_\alpha} \quad (A17)$$

$$z_{S_3}^{nk}(\alpha) = R_{min}\frac{\varepsilon_1(E_1 - E_2) + \varepsilon_4(E_5 - E_4)}{(R_{min}/R_\alpha)/(E_5 - E_{nk}) - (E_2 - E_{nk})} \quad (A18)$$

The integral must be zero if strains outside the Class III limits (ε_g to ε_2) occur, so we define

$$z_3^{nk} = \min[\max(z_{S_3}^{nk}(\alpha), z_{nk}], z_{n,k+1} \quad \text{(A19)}$$

with

$$z_{nk} = \frac{(n-k-1)z_{0g} + kz_{02}}{n-1}, \; k = 0 \ldots n-1 \quad \text{(A20)}$$

Here, z_{nk} represents integration limits between the n groups defined earlier.

Another decomposition of the integral at the z coordinate corresponding to ε_4 is necessary, because the integrand changes discontinuously there. This limit is defined as z_z^{nk}. Additionally, z_z^{nk} has to be restricted to the interval $[z_3^{nk}, z_{n,k+1}]$ if case (a) holds, and $[z_{nk}, z_3^{nk}]$ if case (b) holds (see below).

After these preliminary definitions, the Class III bending moment can be evaluated. Again, case (a) or case (b) may occur, depending on the choice of elasticity parameters. However, if one case holds for a single group, it holds for all other groups as well.

Case (a)

$$\begin{aligned} M_{\mathrm{III}} &= \int_{z_{0g}}^{z_{02}} I^{\mathrm{III}} \\ &= \sum_{k=0}^{n-1} \left[\int_{z_{nk}}^{z_3^{nk}} I_1^{\mathrm{III}} \text{ (branch from } \varepsilon_{\max} \text{ to } S_3^{nk}) \right. \\ &\quad \left. + \int_{z_3^{nk}}^{zz_{nk}} I_2^{\mathrm{III}}(S_3^{nk} \text{ to } \varepsilon_4) + \int_{z_{nk}}^{zz_{n,k+1}} I_3^{\mathrm{III}}(\varepsilon_4 \text{ to } 0) \right] \end{aligned} \quad \text{(A21)}$$

with

$$z_z^{nk} \equiv \min[\max(z_3^{nk}, \varepsilon_4 R_\alpha), z_{n,k+1}] \quad \text{(A22)}$$

Case (b)

$$\begin{aligned} M_{\mathrm{III}} &= \int_{z_{0g}}^{z_{02}} I^{\mathrm{III}} \\ &= \sum_{k=0}^{n-1} \left[\int_{z_{nk}}^{zz_{nk}} I_3^{\mathrm{III}} \text{ (branch from } \varepsilon_4 \text{ to } 0) \right. \\ &\quad + \int_{zz_{nk}}^{z_3^{nk}} I_2^{\mathrm{III}}(S_3^{nk} \text{ to } \varepsilon_4) \\ &\quad \left. + \int_{z_3^{nk}}^{zz_{n,k+1}} I_1^{\mathrm{III}}(\varepsilon_{\max} \text{ to } S_3^{nk}) \right] \end{aligned} \quad \text{(A23)}$$

with

$$z_z^{nk} \equiv \min[\max(z_3^{nk}, \varepsilon_4 R_\alpha), z_{n,k+1}] \quad \text{(A24)}$$

The corresponding stress expressions are given by

$$\begin{aligned} I_1^{\mathrm{III}}: \sigma_1^{\mathrm{III}} &= \varepsilon_1 E_1 + (\varepsilon_{\max} - \varepsilon_1) E_2 \\ &\quad - (\varepsilon_{\max} - \varepsilon) E_{nk} \end{aligned} \quad \text{(A25)}$$

$$I_2^{\mathrm{III}}: \sigma_2^{\mathrm{III}} = \varepsilon_4 E_4 + (\varepsilon - \varepsilon_4) E_5 \quad \text{(A26)}$$

$$I_3^{\mathrm{III}}: \sigma_3^{\mathrm{III}} = \varepsilon E_4 \quad \text{(A27)}$$

so we finally have

Case (a)

$$\begin{aligned} M_{\mathrm{III}}(\alpha) &= 2b \sum_{k=0}^{n-1} \left[\varepsilon_1 (E_1 - E_2) \frac{(z_3^{nk})^2 - z_{nk}^2}{2} \right. \\ &\quad \left. + (E_2 - E_{nk}) \frac{(z_3^{nk})^3 - z_{nk}^3}{3R_{\min}} + E_{nk} \frac{(z_3^{nk})^3 - z_{nk}^3}{3R_\alpha} \right] \\ &\quad + 2b \sum_{k=0}^{n-1} \left[E_4 \frac{(z_z^{nk})^3 - (z_3^{nk})^3}{3R_\alpha} + \varepsilon_4 (E_4 - E_5) \right. \\ &\quad \left. \times \frac{z_{n,k+1}^2 - (z_z^{nk})^2}{2} + E_5 \frac{z_{n,k+1}^3 - (z_z^{nk})^3}{3R_\alpha} \right] \end{aligned} \quad \text{(A28)}$$

Case (b)

$$\begin{aligned} M_{\mathrm{III}}(\alpha) &= 2b \sum_{k=0}^{n-1} \left[\varepsilon_1 (E_1 - E_2) \frac{z_{n,k+1}^2 - (z_3^{nk})^2}{2} \right. \\ &\quad + (E_2 - E_{nk}) \frac{z_{n,k+1}^3 - (z_3^{nk})^3}{3R_{\min}} \\ &\quad \left. + E_{nk} \frac{z_{n,k+1}^3 - (z_3^{nk})^3}{3R_\alpha} \right] \\ &\quad + 2b \sum_{k=0}^{n-1} \left[E_4 \frac{(z_z^{nk})^3 - z_{nk}^3}{3R_\alpha} + \varepsilon_4 (E_4 - E_5) \right. \\ &\quad \left. \times \frac{(z_3^{nk})^2 - (z_z^{nk})^2}{2} + E_5 \frac{(z_3^{nk})^3 - (z_z^{nk})^3}{3R_\alpha} \right] \end{aligned} \quad \text{(A29)}$$

A.4. Class IV (fibres of maximum strain greater than ε_1)

The unloading branch for Class IV fibres runs with a uniform slope of E_6 from maximum strain towards the lower plateau which it intersects at a strain S_4 and continues along the plateau (E_5) to the point ε_4. It decreases with a slope of E_4 back to the origin (Fig. 5d).

The stress/strain mesh yielding, S_4, is given by

$$\begin{aligned} &\varepsilon_1 E_1 + (\varepsilon_2 - \varepsilon_1) E_2 + (\varepsilon_{\max} - \varepsilon_2) E_3 \\ &\quad = \varepsilon_4 E_4 + (S_4 - \varepsilon_4) E_5 + (\varepsilon_{\max} - S_4) E_6 \end{aligned} \quad \text{(A30)}$$

or

$$S_4 = \frac{(z/R_{\min})(E_3 - E_6) + \varepsilon_1(E_1 - E_2) + \varepsilon_2(E_2 - E_3) + \varepsilon_4(E_5 - E_4)}{E_5 - E_6} \quad \text{(A31)}$$

The corresponding z coordinate becomes

$$z_{S_4}(\alpha) = R_{\min} \frac{\varepsilon_1(E_1 - E_2) + \varepsilon_2(E_2 - E_3) + \varepsilon_4(E_5 - E_4)}{(R_{\min}/R_\alpha)(E_5 - E_6) - (E_3 - E_6)} \quad \text{(A32)}$$

Class IV strain should be limited to the interval (ε_2, ε_{max}) suggesting the definition

$$z_4 = \min[\max z_{S_4}(\alpha), z_{02}], h/2 \qquad \text{(A33)}$$

Like in Class III, the integrand changes discontinuously at ε_4, so the integral has to be split at the corresponding z coordinate. This splitting point is defined as z_2 and is restricted to the interval (z_{02}, z_4) if case (a) holds (fibres with higher z coordinates reach S_2 first, lower z fibres follow), or (z_4, $h/2$) if case (b) holds (fibres with lower z coordinates reach S_2 first, higher z fibres follow). Consequently, the moment integral of class IV is given by

Case (a)

$$M_{IV} = \int_{z_{02}}^{h/2} I^{IV} = \int_{z_{02}}^{z_4} I_1^{IV} \text{ (branch from } \varepsilon_{max} \text{ to } S_4)$$
$$+ \int_{z_4}^{z_z} I_2^{IV}(S_4 \text{ to } \varepsilon_4) + \int_{z_z}^{h/2} I_3^{IV}(\varepsilon_4 \text{ to } 0) \qquad \text{(A34)}$$

with

$$z_z \equiv \min[\max(z_{02}, \varepsilon_4 R_\alpha), z_4] \qquad \text{(A35)}$$

Case (b)

$$M_{IV} = \int_{z_{02}}^{h/2} I^{IV} = \int_{z_{02}}^{z_2} I_3^{IV} \text{ (branch from } \varepsilon_4 \text{ to } 0)$$
$$+ \int_{z_z}^{z_4} I_2^{IV}(S_4 \text{ to } \varepsilon_4) + \int_{z_4}^{h/2} I_1^{IV}(\varepsilon_{max} \text{ to } S_4) \qquad \text{(A36)}$$

with

$$z_z \equiv \min[\max(z_4, \varepsilon_4 R_\alpha), h/2] \qquad \text{(A37)}$$

The following stress expressions have to be inserted into the integrands:

$$I_1^{IV}: \sigma_1^{IV} = \varepsilon_1 E_1 + (\varepsilon_2 - \varepsilon_1)E_2 + (\varepsilon_{max} - \varepsilon_2)E_3 - (\varepsilon_{max} - \varepsilon)E_6 \qquad \text{(A38)}$$

$$I_2^{IV}: \sigma_2^{IV} = \varepsilon_4 E_4 + (\varepsilon_{max} - \varepsilon_4)E_5 \qquad \text{(A39)}$$

$$I_3^{IV}: \sigma_3^{IV} = \varepsilon E_4 \qquad \text{(A40)}$$

The final result yields

Case (a)

$$M_{IV}(\alpha) = 2b\left\{[\varepsilon_1(E_1 - E_2) + \varepsilon_2(E_2 - E_3)]\frac{z_4^2 - z_{02}^2}{2} + (E_3 - E_6)\frac{z_4^3 - z_{02}^3}{3R_{min}} + E_6\frac{z_4^3 - z_{02}^3}{3R_\alpha}\right\}$$
$$+ 2b\left[E_4\frac{z_z^3 - z_4^3}{3R_\alpha} + \varepsilon_4(E_4 - E_5) \times \frac{(h^2/4) - z_z^2}{2} + E_5\frac{(h^3/8) - z_z^3}{3R_\alpha}\right] \qquad \text{(A41)}$$

Case (b)

$$M_{IV}(\alpha) = 2b\left\{[\varepsilon_1(E_1 - E_2) + \varepsilon_2(E_2 - E_3)] \times \frac{(h^2/4) - z_4^2}{2} + (E_3 - E_6) \times \frac{(h^3/8) - z_4^3}{3R_{min}} + E_6\frac{(h^3/8) - z_4^3}{3R_\alpha}\right\}$$
$$+ 2b\left[E_4\frac{z_z^3 - z_{02}^3}{3R_\alpha} + \varepsilon_4(E_4 - E_5)\frac{z_4^2 - z_z^2}{2} + E_5\frac{z_4^3 - z_z^3}{3R_\alpha}\right] \qquad \text{(A42)}$$

The total bending moment during the unloading process is the sum over all contributions of Classes I–IV

$$M(\alpha) = M_I(\alpha) + M_{II}(\alpha) + M_{III}(\alpha) + M_{IV}(\alpha) \qquad \text{(A43)}$$

References

1. F. E. WANG, B. F. DESAVAGE and W. J. BUEHLER, *J. Appl. Phys.* **39** (1968) 2166.
2. W. J. BUEHLER and F. E. WANG, *Ocean Eng.* **1** (1968) 105.
3. P. HAASEN, in "Physikalische Metallkunde" (Springer, Berlin, Heidelberg, New York, Tokyo, 1984) p. 266.
4. L. DELAEY, R. V. KRISHNAN, H. TAS and H. WARLIMONT, *J. Mater. Sci.* **9** (1974) 1521.
5. F. ÖLANDER, *Z. Krist.* **83A** (1932) 145.
6. M. W. BURKART and T. A. READ, *Trans. AIME* **197** (1953) 1516.
7. L. C. CHANG and T. A. READ, *ibid.* **191** (1951) 47.
8. P. TAUTZENBERGER and D. STÖCKEL, *Z. Wirtsch. Fertigung* **81** (1986) 703.
9. E. HORNBOGEN, *Metallwiss. Techn.* **41** (1987) 488.
10. P. H. ADLER, W. YU, A. R. PELTON, R. ZADNO, T. W. DUERIG and R. BARRESI, *Scripta Metall.* **24** (1990) 943.
11. R. PLIETSCH, Diploma Thesis, University of Bonn (1993).
12. D. STÖCKEL, in "Legierungen mit Formgedächtnis", edited by D. Stöckel and E. Hombogen (Expert, Ehningen, 1988) p. 31.
13. J. W. CHRISTIAN and D. E. LAUGHLIN, *Scripta Metall.* **21** (1987) 1131.
14. I. MÜLLER, *Phys. Bl.* **44** (1988) 135.
15. S. BRANDT, "Datenanalyse" (BI Wissenschaftsverlag, Heidelberg, 1989).
16. D. W. MARQUARDT, *J. Soc. Ind. Appl. Mathem.* **11** (1963) 431.
17. C. BOURAUEL, L. NOLTE and D. DRESCHER, *Biomed. Technol.* **37** (1992) 46.
18. D. DRESCHER, C. BOURAUEL and M. THIER, *Eur. J. Orthodont.* **13** (1991) 169.

Received 16 September 1993
and accepted 16 May 1994